doi:10.1016/j.jmb.2012.07.004 J. Mol. Biol. (2012) 423, 249–256

Contents lists available at www.sciencedirect.com

Journal of Molecular Biology

journal homepage: http://ees.elsevier.com.jmb

High-Speed Atomic Force Microscopy: Cooperative Adhesion and Dynamic Equilibrium of Junctional Microdomain Membrane Proteins

Adai Colom[1], Ignacio Casuso[1], Thomas Boudier[2] and Simon Scheuring[1]*

[1]*U1006 INSERM, Aix-Marseille Université, Parc Scientifique de Luminy, Marseille F-13009, France*
[2]*Université Pierre et Marie Curie, 7 Quai Saint Bernard, Paris F-75252, France*

Received 7 May 2012;
received in revised form
29 June 2012;
accepted 3 July 2012
Available online
14 July 2012

Edited by J. Bowie

Keywords:
atomic force microscopy;
high-speed atomic force microscopy;
aquaporin;
connexin;
lens membrane

Junctional microdomains, paradigm for membrane protein segregation in functional assemblies, in eye lens fiber cell membranes are constituted of lens-specific aquaporin-0 tetramers ($AQP0_4$) and connexin (Cx) hexamers, termed connexons. Both proteins have double function to assure nutrition and mediate adhesion of lens cells. Here we use high-speed atomic force microscopy to examine microdomain protein dynamics at the single-molecule level. We found that the adhesion function of head-to-head associated $AQP0_4$ and Cx is cooperative. This finding provides first experimental evidence for the mechanistic importance for junctional microdomain formation. From the observation of lateral association–dissociation events of $AQP0_4$, we determine that the enthalpic energy gain of a single $AQP0_4$–$AQP0_4$ interaction in the membrane plane is -2.7 k_BT, sufficient to drive formation of microdomains. Connexon association is stronger as dynamics are rarely observed, explaining their rim localization in junctional microdomains.

Introduction

The eye lens is a transparent biological marble of tightly stacked cells. The dense cell packing, the absence of the major organelles inside the cells, and the avascular nature of the lens tissue assure its transparency throughout life. In order to maintain lens cells metabolically active and to assure cell–cell interactions, channels and adhesion proteins evolved in lens cell membranes that nourish lens cells and adhere at short distances.

Aquaporin-0 tetramers ($AQP0_4$) and connexins (Cx) are major intrinsic proteins in the membranes and comprise about 60% and 15%, respectively, of the total amount of membrane protein. $AQP0_4$ form stable tetramers, while Cx form hexamers termed connexons. $AQP0_4$ and connexons mediate solute transport (water, ions, metabolites and waste) and, thus, are responsible for the lens microcirculation system crucial for maintaining cells nativeness and, hence, lens transparency.[1] Malfunction of both proteins results in cataract.[2,3] The channels assemble together in junctional microdomains[4,5] in the plasma membrane of eye lens fiber cells. It has been revealed that the assembly of $AQP0_4$ and Cx in junctional microdomains is mediated by interaction of their cytoplasmic loops.[6] Importantly, high-resolution electron crystallography of $AQP0_4$ showed annular lipids surrounding $AQP0_4$[7] in junctional microdomains, indicating a membrane-mediated interaction mechanism in the lateral $AQP0_4$–$AQP0_4$ assembly process. Indeed, different types of lipids can occupy specific regions on the $AQP0_4$ surface and intercalate between $AQP0_4$.[8] Junctional microdomains have typically the size of

**Corresponding author.* E-mail address: simon.scheuring@inserm.fr.

Abbreviations used: HS-AFM, high-speed atomic force microscopy; 2D, two dimensional.

a few thousands of square nanometers of tetragonal arranged $AQP0_4$ edged or neighbored by Cx.[9] It has been proposed that the fluid flow across lens cell membranes might be promoted by the tight association of the channel proteins.[2]

Beyond channeling function, both $AQP0_4$ and Cx form stable head-to-head associations with equivalent proteins in the membrane of the neighboring cell by means of their extracellular loops.[9,10] This secondary function as cell adhesion molecules[6] was structurally first characterized in two-dimensional (2D) crystals of purified proteins of $AQP0_4$[11] and connexons[12] and is now described to atomic resolution for both proteins.[7,13] The adhesion junctions formed imply short extracellular loops, explaining why these molecules are able to provide such a tight and short-distance cell packing.[7,13] Early thin-section electron microscopy studies of lens cells showed $AQP0_4$ and Cx in thin and thick junctions, depending on the separation distance between cell membranes, usually termed thin junction for $AQP0_4$ and gap junction for Cx.[5] Using atomic force microscope force spectroscopy, we have measured the adhesive strength of the Cx extracellular loop-2, showing it to support important pulling forces.[14]

Hence, while the structure of the junctional microdomain is well described and while the structure, function, and adhesion capability of the individual proteins is assessed, essentially nothing is known about the lateral assembly dynamics and adhesion properties of the components in junctional microdomains. This is regrettable as it is the dynamics, the lateral assembly, and the adhesion association strength between the molecules that allow the microdomains to be formed and to maintain their integrity in the cell membranes. Furthermore, to date, there is no concise explanation what the advantage for the molecules to associate in junctional microdomains rather than being randomly distributed in the cell membrane is, specifically if this architecture has impact on the secondary adhesion function.

In order to answer these questions, we used high-speed atomic force microscopy (HS-AFM) to analyze the dynamics of $AQP0_4$ and Cx in real time in the native lens cell membrane. We are able to determine the dynamics of $AQP0_4$ and energetics of their interaction and simulate how these two parameters are crucial and sufficient for maintaining $AQP0_4$ in a dynamic equilibrium in junctional arrays. We also show, for the first time, that the proteins in junctional microdomains reveal adhesion cooperativity tying together neighboring membranes as one large adhesion element.

Results

When purifying membranes from lens cells, junctional microdomains remain intact[2,9] as reflected by an upper membrane layer sticking on a lower membrane (Fig. 1a). AFM has the considerable advantage over other imaging techniques that it allows manipulation of the sample under investigation. In particular, HS-AFM[15] in contact mode[16] enabled us to mechanically dissect[17,18] junctional microdomains (Fig. 1; Supplementary Movie 1). Indeed, initially, the upper membrane layer exposing the cytoplasmic face is observed. Protein domains (Fig. 1a, $t = 0.0$ s, labels 1 and 2) that pair with protein domains in the underlying layer exposing the extracellular face upwards (Fig. 1a, $t = 70.5$ s, labels 1 and 2) can be distinguished within the upper membrane layer. The proteins involved are $AQP0_4$ and connexons (Fig. 1a, $t = 70.5$ s, inset; Supplementary Movie 2). Contact-mode HS-AFM imaging and nano-dissection[2,9,11,16] (Fig. 1a) allowed us to qualitatively detect cooperativity of adhesion of the junctional proteins by measuring the area and perimeter of the upper adhering junctional microdomain layer during removal. Surprisingly, this analysis showed that the upper layer was attached in entities of distinct area of about 10,000 nm^2 (100 nm × 100 nm) area — reflected as plateaus in area *versus* time graph (Fig. 1b). Such a surface area typically corresponds to about 250 $AQP0_4$ and connexon hexamers, in agreement with previous structural description of junctional microdomains with $AQP0_4$ of coherent orientation[19,20] (Fig. 2a). Averaging of the movie frames recorded during the duration of a stable microdomain association during dissection (plateaus in the area *versus* time graph) allows picturing the morphology of microdomain adhesion entities (Fig. 1b, insets). Clearly, the adhesion function of the junctional microdomain proteins is cooperative, in contrast to a linear relationship between adhesive area *versus* time expected for a dissection where the proteins do not act with cooperativity. Previously, we have shown that the extracellular loop-2 of Cx supports important pulling forces.[14] Here we show that, in order to create adhesive junctions that are strong and of long lifetime to assure cell packing for lens transparency, $AQP0_4$ and Cx work together. This shades a completely novel light on the necessity of these proteins to form junctional microdomains, probably not for solute channeling but as cooperative adhesion platforms.

Using HS-AFM in oscillating mode, we have been able to acquire highly contrasted overview images of the supramolecular assembly of $AQP0_4$ and connexons in junctional microdomains (Fig. 2a; Supplementary Movie 3). The movie reports $AQP0_4$ in ordered arrays, partially edged by connexons. The $AQP0_4$ arrays have lattice parameters of $a = b = 65$ Å and $\gamma = 90°$, alike the packing in junctional 2D crystals.[7,21] Connexons edge $AQP0_4$ arrays, sometimes separate arrays of different orientation and are non-ordered (Fig. 2a), as previously reported.[9] HS-

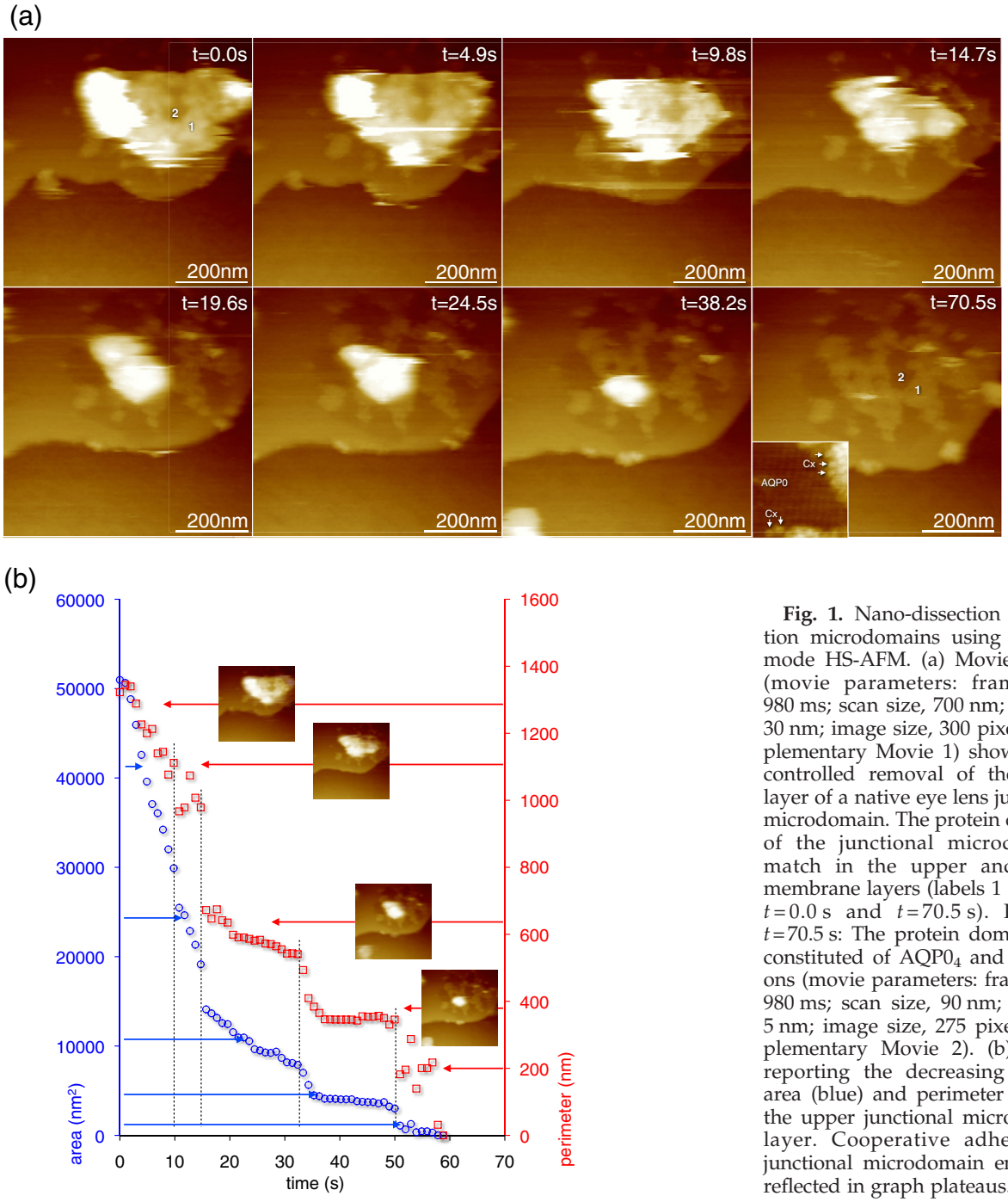

Fig. 1. Nano-dissection of junction microdomains using contact-mode HS-AFM. (a) Movie frames (movie parameters: frame rate, 980 ms; scan size, 700 nm; *z*-range, 30 nm; image size, 300 pixels; Supplementary Movie 1) showing the controlled removal of the upper layer of a native eye lens junctional microdomain. The protein domains of the junctional microdomains match in the upper and lower membrane layers (labels 1 and 2 in $t = 0.0$ s and $t = 70.5$ s). Inset in $t = 70.5$ s: The protein domains are constituted of $AQP0_4$ and connexons (movie parameters: frame rate, 980 ms; scan size, 90 nm; *z*-range, 5 nm; image size, 275 pixels; Supplementary Movie 2). (b) Graph reporting the decreasing surface area (blue) and perimeter (red) of the upper junctional microdomain layer. Cooperative adhesion of junctional microdomain entities is reflected in graph plateaus.

AFM observation of the junctional microdomains shows tetramer movements at edges and in between individual arrays. Zooming into areas of interest, molecules assembling and disassembling from the array edges can be observed (Fig. 2b and c; Supplementary Movies 4 and 5).

The structure of the $AQP0_4$ assembly in junctional microdomains and of structurally similar 2D crystals have been resolved to high and atomic resolution by AFM[9] and electron crystallography,[7] respectively. Despite this wealth of structural information, there is essentially nothing known about the assembly and disassembly process of $AQP0_4$ in arrays and its energetic grounds. In more general terms, the understanding of the assembly of membrane proteins in functional domains (detergent-resistant membranes and rafts) is of key importance in cell biology.[22–24] HS-AFM at 250 ms frame rate of an

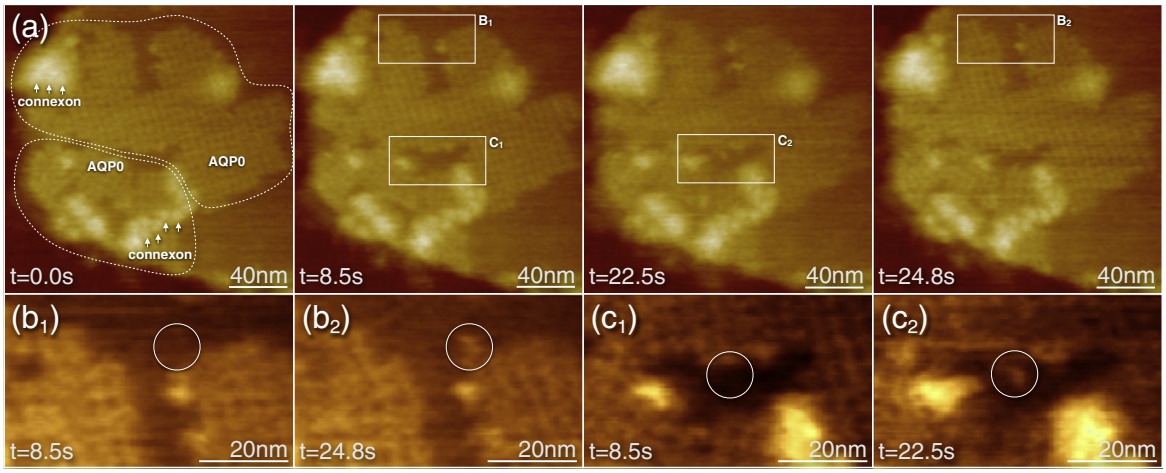

Fig. 2. The supramolecular assembly of $AQP0_4$ and connexons in junctional eye lens membranes analyzed using oscillating mode HS-AFM. (a) Movie frames (movie parameters: frame rate, 776 ms; scan size, 200 nm; *z*-range, 18 nm; image size, 300 pixels; Supplementary Movie 3) showing two native tetragonal $AQP0_4$ arrays (outlines in $t = 0.0$ s), in vicinity of non-ordered connexons. Molecular movement can be observed at array borders (outline B; Supplementary Movie 4) and in between arrays (outline C; Supplementary Movie 5). (b and c) Magnified views of outlines in (a) with structural changes observed on array edges outlined by circles.

$AQP0_4$ microdomain border allowed us to analyze quantitatively the association and dissociation of $AQP0_4$ (Fig. 3; Supplementary Movie 6). Array expansion (Fig. 3a, $t = 0$–2.50 s) and retraction (Fig. 3a, $t = 2.50$–3.25 s) were observed, due to recruitment and liberation of diffusing $AQP0_4$ in the lens cell membrane. $AQP0_4$ positions have been determined[25] in the movie frames and the tetramers assigned to five groups depending on the number of direct neighbors (4, 3, 2, 1, or 0) that a tetramer has. Subsequently, dissociation events of $AQP0_4$ from the array were analyzed to determine the lifetime during which the dissociated molecule had been in place and the number of edges it had engaged before leaving the array. We hypothesized that the lifetime of a tetramer in the array is related to the number of neighboring tetramers because the detachment probability is expected to decline exponentially with the number "n" of bonds (occupied edges) a tetramer is attached with, following:

$$\rho_{(\text{dissociation})} = e^{-\left(\frac{n \times E_{(\text{bond})}}{k_B T}\right)} \quad (1)$$

We found the lifetimes $\tau_{(n)}$ (average ± standard deviation), $\tau_{(2)} = 9.8 \pm 0.9$ s and $\tau_{(1)} = 0.7 \pm 1.0$ s, for tetramer with two neighbors and one neighbor, respectively (Fig. 3b); tetramers with three neighbors (along an array border) dissociate so rarely that we could not assess significant statistics, and dissociation of tetramers with four neighbors (inside the array) was never observed. From the residence lifetimes before dissociation of tetramers with two bonds or one bond, the interaction energy of an $AQP0_4$–$AQP0_4$ association could be determined, following:

$$\tau_{(1)} / \tau_{(2)} = e^{\left(\frac{E_{(\text{two bonds})} - E_{(\text{one bond})}}{k_B T}\right)} \quad (2)$$

From the HS-AFM dynamic imaging of the $AQP0_4$ residence lifetimes at the microdomain edge, an interaction potential strength of one $AQP0_4$–$AQP0_4$ association of $-2.7 \pm 0.4\ k_B T$ was determined.

To test the consistency of the data and the accuracy of the $AQP0_4$ array formation rationale, we have employed a 2D Monte Carlo simulation of $AQP0_4$ (Fig. 3c and d). Lacking quantitative knowledge on the adhesion interaction energy between AQP0, our simulation is restricted to one membrane layer. Future computational work might address the double-membrane architecture of the adhesion microdomains.[26] Using the experimentally derived interaction potential well depth of $-2.7\ k_B T$ for one $AQP0_4$–$AQP0_4$ edge association, the probability ρ with which a tetramer moves depending on the number of neighbors is calculated following formula (1). We let 4000 pixels randomly diffuse on a square lattice of area 40,000 pixels, simulating the diffusion of square $AQP0_4$ tetramers in an excess of membrane space able to assemble into square microdomain arrays. After 300,000 simulation steps, the tetramers, initially randomly distributed, have assembled into domains (Fig. 3c, top panels), with a total of 2386 ± 6, 799 ± 14, 448 ± 13, 192 ± 8, and 173 ± 15 tetramers with 4, 3, 2, 1, and 0 occupied edges and an average number of occupied edges of 3.41 ± 0.01 (Fig. 3c, bottom panel; Supplementary

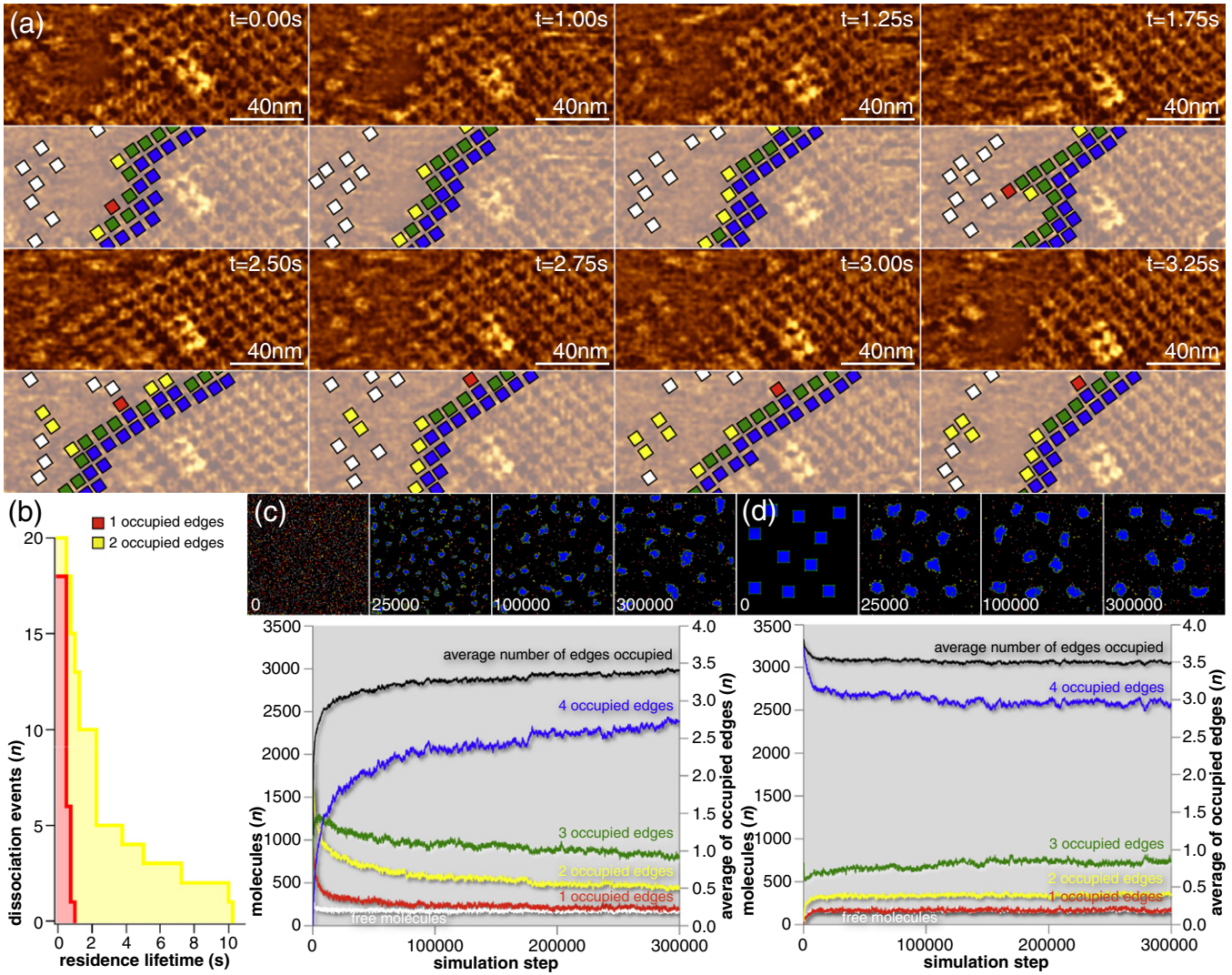

Fig. 3. $AQP0_4$ assembly. (a) Movie frames (movie parameters: frame rate, 250 ms; scan size, 142 nm; *z*-range, 3 nm; image size, 300 × 100 pixels; Supplementary Movie 6) showing native tetragonal $AQP0_4$ arrays assembling ($t = 0$–2.50 s) and disassembling ($t = 2.50$–3.25 s). Bottom panels: Schematic outline of $AQP0_4$ localizations at the array edge; the squares are colored according to the number of bound edges to neighboring tetramer (blue, four edges bound; green, three edges bound; yellow, two edges bound; red, one edge bound; white, zero edge bound or freely diffusing tetramer). (b) Analysis of the number of dissociation events as a function of prior residence lifetime τ, resulting in $\tau_{(2)} = 9.8 \pm 0.9$ s and $\tau_{(1)} = 0.7 \pm 1.0$ s for tetramer with two neighbors and one neighbor, respectively. (c and d) Monte Carlo simulation of $AQP0_4$ array formation starting from random distribution of tetramer (c) or preformed arrays (d) (Supplementary Movies 7 and 8). Bottom panels: Graph analysis of molecule assembly.

Movie 7). In a representative experimental image of an $AQP0_4$ microdomain (see Fig. 2a), 182, 47, 31, and 3 tetramers with 4, 3, 2, and 1 occupied edges and an average number of occupied edges of 3.41 are found (Supplementary Fig. S1). Hence, the ratio of tetramer in characteristic assembly patterns (4, 3, 2, and 1 neighbors) was 1/0.33/0.19/0.08 in the simulation, comparing well to the ratio 1/0.36/0.26/0.03 in the experimental image. Hence, the simulation with a unique parameter, the experimentally defined $AQP0_4$–$AQP0_4$ interaction energy, is able to laterally assemble realistic $AQP0_4$ microdomains (Supplementary Movie 7). To further corroborate the solidity of the rationale, we performed simulations starting from preformed square arrays (Fig. 3d; Supplementary Movie 8). These simulations resulted in 2564 ± 11, 742 ± 9, 353 ± 10, 172 ± 17, and 168 ± 16 tetramers with 4, 3, 2, 1, and 0 occupied edges and an average number of occupied edges of 3.49 ± 0.01. Additionally, the simulations starting from the randomly distributed $AQP0_4$ resulted in domains of 185 ± 85 tetramers, comparable with the size (~250 $AQP0_4$) of the microdomains experimentally assessed. Thus, with the use of $-2.7\ k_BT$ interaction potential strength, simulations converged to similar and realistic results independent of the starting conditions.

Simulations with interaction energies between $AQP0_4$ of $-1.7\ k_BT$ did not form arrays or dissociated preformed arrays. With an interaction strength of $-3.7\ k_BT$, simulations did not converge after 300,000 steps, and resulting arrays did not reveal comparable morphology, that is, neither a similar ratio of tetramer with 4, 3, 2, 1, and 0 occupied edges nor a similar average number of occupied edges, with those imaged by HS-AFM experiment (Supplementary Fig. S1). Simulations using the realistic $-2.7\ k_BT$ interaction potential strength converged also independent on the protein concentration in the membrane. Furthermore, this simulation allowed us to estimate that, with an $AQP0_4$–$AQP0_4$ interaction strength of $-2.7\ k_BT$, about 1% of the membrane is occupied by free tetramer that is in a dynamic equilibrium and associates and dissociates from arrays (Supplementary Fig. S2).

The dynamics of connexon assembly differs from $AQP0_4$ in many ways. First, and most important, connexon assembly appears to be isotropic, and the resulting assembly is non-ordered. Second, connexons dissociate and associate much more rarely. The events are so rare that they are scarcely observed using HS-AFM, prohibiting assessment of quantitative values and modeling (Fig. 4a; Supplementary Movie 9). From hundreds of connexons at assembly edges investigated, we could observe only a handful of them associating or dissociating during HS-AFM inspection at given frame rate (Fig. 4b–d), indicating a strong association potential of connexons. The regular assembly of $AQP0_4$ in square arrays with a dynamic tetramer turnover at free $AQP0_4$ edges, as well as the non-ordered assembly with rare dissociation of connexons, explains the segregation of the two protein species in characteristic junctional microdomains where $AQP0_4$ form square arrays with densely packed connexons at the edges. Fast-associating and fast-dissociating $AQP0_4$, trying to optimize the occupancy of their tetramer surfaces, nucleate and grow junctional microdomains, while associating connexons break the order and periodicity of the $AQP0_4$ array, remain stable, and hinder further $AQP0_4$ assembly to microdomain edges occupied by connexons. Finally, the coupling of $AQP0_4$ and connexons has been shown to enhance gap junction coupling with the neighboring cell.[6]

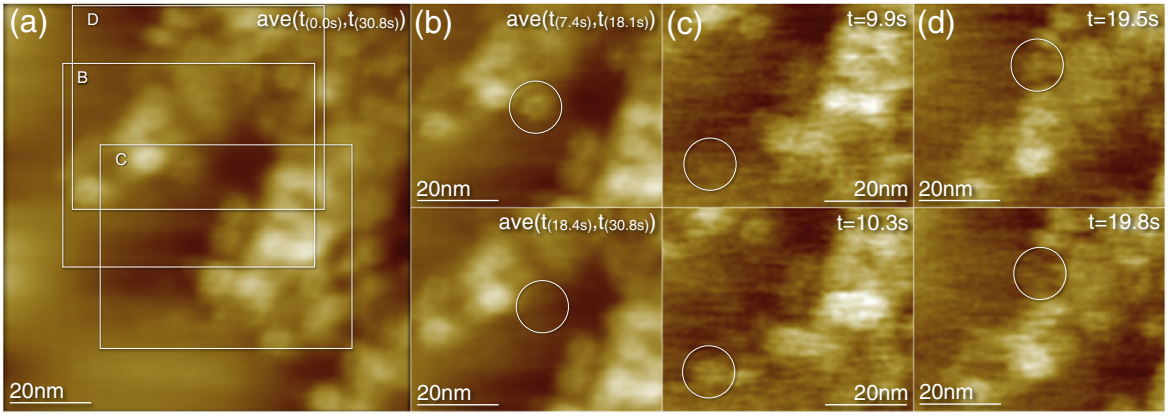

Fig. 4. Connexon assembly. (a) Average over 30.8 s of HS-AFM movie (movie parameters: frame rate, 354 ms; scan size, 100 nm; *z*-range, 4 nm; image size, 300 × 300 pixels; Supplementary Movie 9) showing densely packed connexons. (b) Top panel: Average of frames *t* (7.4 s) to *t* (18.1 s); bottom panel, average of frames *t* (18.4 s) to *t* (30.8 s) displaying the disassembly of a connexon, the six subunits are resolved. (c and d) Individual subsequent image frames showing the assembly (c) and disassembly (d) of connexons.

Therefore, the assembly dynamics and interaction energetics guide the formation of the characteristic architecture of junctional microdomains in which the proteins adhere cooperatively to the neighboring cell, in the course crucial for the maintenance of the lens microcirculation system[1] and thus mammalian vision.

Discussion

High-resolution electron crystallography of junctional $AQP0_4$ resolving the annular lipids showed that $AQP0_4$ is completely surrounded by lipids in the native square arrays.[7,21] 2D crystallization and structure determination of $AQP0_4$ in lipids with different headgroups and acyl-chain length showed that the distance between the headgroup-phosphodiester groups in the two leaflets was quasi identical and that the localization of the acyl-chains on the protein surface is similar, independent of the lipid type.[8] Hence, the lipid association is strongly dictated by the protein to fit its hydrophobic surfaces. Indeed, while the bilayer thickness of annular lipids was determined as ~32 Å,[8] the lens cell membrane is ~46 Å thick.[9] In other words, the junctional microdomain membrane proteins are in a hydrophobic mismatch with the native membrane; therefore, the main component of the interaction potential is membrane mediated.[27] In order to minimize the energetic cost of membrane bending around the channels, $AQP0_4$ and connexons associate in microdomains, potentially a general physical principle for the formation of functional protein associations in cell membranes.[23] HS-AFM imaging of the dissociation probabilities allowed us to determine that the energetic gain of a membrane-mediated protein–protein association is about $-2.7\ k_BT$. In a previous work,[28] the single-bond association energy of bacteriorhodopsin was estimated to be about $-1.5\ k_BT$; bacteriorhodopsin has six nearest neighbors in the characteristic $p3$ 2D crystal. Hence, $AQP0_4$ and bacteriorhodopsin 2D arrays are of comparable stability. Monte Carlo simulations showed that the formation and the dynamic equilibrium are particularly sensitive to the energetic term of the interaction. Smaller interaction energy ($+1\ k_BT$) was insufficient to drive microdomain formation, while higher interaction energy ($-1\ k_BT$) resulted in aggregates of a few molecules in simulations. Our simulation is in the framework of the theory of Ostwald ripening in 2D,[29] a first-order phase transition model where $AQP0_4$ are either bound or free. Hence, the average radius $\langle R \rangle$ of the clusters evolves in time t following $\langle R \rangle \sim (t/\ln t)^{1/3}$, going asymptotically toward a stable cluster size.

Testing different protein concentrations and starting conditions gave us additional confidence in the importance of the membrane-mediated energy term of interaction. Future experiments may analyze the interaction behavior of AQP1, an aquaporin closely related to AQP0, which is not known to form junctional microdomains.[30]

The existence of junctional microdomains has been reported early by electron microscopy techniques.[20] The channel function that is mediated by each single molecule of both protein species, $AQP0_4$ and connexons, does not provide explanation concerning the advantage that is provided by the formation of the microdomains. Here we show, using the AFM tip as a nano-manipulator, that the $AQP0_4$ and connexon adhesion function in thin and gap junctions is cooperative, providing evidence that microdomain formation is crucial for tight cell–cell adhesion and, hence, for the structural integrity of the lens tissue.

Materials and Methods

Lens membrane preparation

Lens membranes have been prepared from sheep lens fiber cells after careful removal of the cortical cells as previously described.[9,31] The cells were broken using a homogenizer in buffer solution [10 mM Tris–HCl (pH 8.0), 5 mM ethylene glycol bis(β-aminoethyl ether) *N*,*N*′-tetraacetic acid, 5 mM ethylenediaminetetraacetic acid, and protease inhibitor] for 5 min, followed by centrifugation (220,000*g*) for 30 min, and the pellet was collected. Membranes were washed first during a homogenizer step in 4 M urea, pH 8.0, and second in 20 mM NaOH, pH 12.0; each time, the membranes are collected again during a centrifugation step at 220,000*g* for 30 min. The pellet is again homogenized in 10 mM Tris–HCl at pH 7.4, followed with the last centrifugation step (300,000*g*) for 60 min to collect the pellet. Finally, the membrane pellet is softly homogenized in stocking buffer 10 mM Tris (pH 7.4).

High-speed atomic force microscopy

An HS-AFM[15] equipped with 8-μm-long cantilevers (spring constant $k = 0.2$ N/m and resonance frequency $f_{(r)} = 700$ kHz; NanoWorld, Neuchâtel, Switzerland) was used for image acquisition shown in Fig. 3 or that equipped with 6-μm-long cantilevers (spring constant $k = 0.1$ N/m and resonance frequency $f_{(r)} = 600$ kHz; Olympus, Japan) was used for image acquisition shown in Figs. 1, 2, and 4. Optimized HS-AFM electronics were used to pilot the dynamic feedback circuit.[32] The imaging scan rates and detailed movie parameters are indicated in the figure and supplementary movie captions.

Data analysis

The data were analyzed using a devoted JAVA-based HS-AFM image analysis and treatment package[25] integrated in the ImageJ image analysis platform.[33]

Supplementary data to this article can be found online at http://dx.doi.org/10.1016/j.jmb.2012.07.004

References

1. Donaldson, P., Kistler, J. & Mathias, R. T. (2001). Molecular solutions to mammalian lens transparency. *Physiology*, **16**, 118–123.
2. Buzhynskyy, N., Girmens, J.-F., Faigle, W. & Scheuring, S. (2007). Human cataract lens membrane at subnanometer resolution. *J. Mol. Biol.* **374**, 162–169.
3. Shiels, A. & Bassnett, S. (1996). Mutations in the founder of the MIP gene family underlie cataract development in the mouse. *Nat. Genet.* **12**, 212–215.
4. Zampighi, G. A., Eskandari, S., Hall, J. E., Zampighi, L. & Kreman, M. (2002). Micro-domains of AQP0 in lens equatorial fibers. *Exp. Eye Res.* **75**, 505–519.
5. Zampighi, G. A., Hall, J. E., Ehring, G. R. & Simon, S. A. (1989). The structural organization and protein composition of lens fiber junctions. *J. Cell Biol.* **108**, 2255–2275.
6. Liu, J., Xu, J., Gu, S., Nicholson, B. J. & Jiang, J. X. (2011). Aquaporin 0 enhances gap junction coupling via its cell adhesion function and interaction with connexin 50. *J. Cell Sci.* **124**, 198–206.
7. Gonen, T., Cheng, Y., Sliz, P., Hiroaki, Y., Fujiyoshi, Y., Harrison, S. C. & Walz, T. (2005). Lipid-protein interactions in double-layered two-dimensional AQP0 crystals. *Nature*, **438**, 633–638.
8. Hite, R. K., Li, Z. & Walz, T. (2010). Principles of membrane protein interactions with annular lipids deduced from aquaporin-0 2D crystals. *EMBO J.* **29**, 1652–1658.
9. Buzhynskyy, N., Hite, R. K., Walz, T. & Scheuring, S. (2007). The supramolecular architecture of junctional microdomains in native lens membranes. *EMBO Rep.* **8**, 51–55.
10. Engel, A., Fujiyoshi, Y., Gonen, T. & Walz, T. (2008). Junction-forming aquaporins. *Curr. Opin. Struct. Biol.* **18**, 229–235.
11. Fotiadis, D., Hasler, L., Müller, D. J., Stahlberg, H., Kistler, J. & Engel, A. (2000). Surface tongue-and-groove contours on lens MIP facilitate cell-to-cell adherence. *J. Mol. Biol.* **300**, 779–789.
12. Unger, V. M., Kumar, N. M., Gilula, N. B. & Yaeger, M. (1999). Three-dimensional structure of a recombinant gap junction membrane channel. *Science*, **283**, 1176–1180.
13. Maeda, S., Nakagawa, S., Suga, M., Yamashita, E., Oshima, A., Fujiyoshi, Y. & Tsukihara, T. (2009). Structure of the connexin 26 gap junction channel at 3.5 Å resolution. *Nature*, **458**, 597–602.
14. Rico, F., Oshima, A., Hinterdorfer, P., Fujiyoshi, Y. & Scheuring, S. (2011). Two-dimensional kinetics of inter-connexin interactions from single-molecule force spectroscopy. *J. Mol. Biol.* **412**, 72–79.
15. Ando, T., Kodera, N., Takai, E., Maruyama, D., Saito, K. & Toda, A. (2001). A high-speed atomic force microscope for studying biological macromolecules. *Proc. Natl Acad. Sci. USA*, **98**, 12468–12472.
16. Casuso, I., Kodera, N., Le Grimellec, C., Ando, T. & Scheuring, S. (2009). Contact-mode high-resolution high-speed atomic force microscopy movies of the purple membrane. *Biophys. J.* **97**, 1354–1361.
17. Scheuring, S., Seguin, J., Marco, S., Levy, D., Robert, B. & Rigaud, J. L. (2003). Nanodissection and high-resolution imaging of the *Rhodopseudomonas viridis* photosynthetic core complex in native membranes by AFM. *Proc. Natl Acad. Sci. USA*, **100**, 1690–1693.
18. Scheuring, S., Sturgis, J. N., Prima, V., Bernadac, A., Levy, D. & Rigaud, J. L. (2004). Watching the photosynthetic apparatus in native membranes. *Proc. Natl Acad. Sci. USA*, **101**, 11293–11297.
19. Buzhynskyy, N., Sens, P., Behar-Cohen, F. & Scheuring, S. (2011). Eye lens membrane junctional microdomains: a comparison between healthy and pathological cases. *New J. Phys.* **13**, 085016.
20. Zampighi, G., Simon, S. A., Robertson, J. D., McIntosh, T. J. & Costello, M. J. (1982). On the structural organization of isolated bovine lens fiber junctions. *J. Cell Biol.* **93**, 175–189.
21. Scheuring, S., Buzhynskyy, N., Jaroslawski, S., Goncalves, R. P., Hite, R. K. & Walz, T. (2007). Structural models of the supramolecular organization of AQP0 and connexons in junctional microdomains. *J. Struct. Biol.* **160**, 385–394.
22. Simons, K. & Ikonen, E. (1997). Functional rafts in cell membranes. *Nature*, **387**, 569–572.
23. Engelman, D. M. (2005). Membranes are more mosaic than fluid. *Nature*, **438**, 578–580.
24. Lajoie, P., Goetz, J. G., Dennis, J. W. & Nabi, I. R. (2009). Lattices, rafts, and scaffolds: domain regulation of receptor signaling at the plasma membrane. *J. Cell Biol.* **185**, 381–385.
25. Husain, M., Boudier, T., Paul-Gilloteaux, P., Casuso, I. & Scheuring, S. (2011). Software for drift compensation, particle tracking and particle analysis of high-speed atomic force microscopy image series. *J. Mol. Recognit.* **25**, 292–298.
26. Wu, Y., Vendome, J., Shapiro, L., Ben-Shaul, A. & Honig, B. (2011). Transforming binding affinities from three dimensions to two with application to cadherin clustering. *Nature*, **475**, 510–513.
27. Casuso, I., Sens, P., Rico, F. & Scheuring, S. (2010). Experimental evidence for membrane-mediated protein–protein interaction. *Biophys. J.* **99**, L47–L49.
28. Yamashita, H., Voïtchovsky, K., Uchihashi, T., Contera, S. A., Ryan, J. F. & Ando, T. (2009). Dynamics of bacteriorhodopsin 2D crystal observed by high-speed atomic force microscopy. *J. Struct. Biol.* **167**, 153–158.
29. Rogers, T. M. & Desai, R. C. (1989). Numerical study of late-stage coarsening for off-critical quenches in the Cahn–Hilliard equation of phase separation. *Phys. Rev. B: Condens. Matter Mater. Phys.* **39**, 11956–11964.
30. Varadaraj, K., Kumari, S. S. & Mathias, R. T. (2010). Transgenic expression of AQP1 in the fiber cells of AQP0 knockout mouse: effects on lens transparency. *Exp. Eye Res.* **91**, 393–404.
31. Gonen, T., Cheng, Y., Kistler, J. & Walz, T. (2004). Aquaporin-0 membrane junctions form upon proteolytic cleavage. *J. Mol. Biol.* **342**, 1337–1345.
32. Kodera, N., Sakashita, M. & Ando, T. (2006). Dynamic proportional-integral-differential controller for high-speed atomic force microscopy. *Rev. Sci. Instrum.* **77**, 083704–083707.
33. Rasband, W. S. (1997–2011). ImageJ U. S. National Institutes of Health, Bethesda, Maryland, USA; http://rsbweb.nih.gov/ij/.